

# LOTR: Face Landmark Localization Using Localization Transformer

Ukrit Watchareeruetai\*    Benjaphan Sommanna    Sanjana Jain    Pavit Noinongyao  
Ankush Ganguly    Aubin Samacoits    Samuel W.F. Earp

**Sertis Vision Lab**

597/5 Sukhumvit Road, Watthana, Bangkok, 10110, Thailand

Nakarin Srirakool†

**Faculty of Science, Chulalongkorn University**

Phayathai Road, Pathum Wan, Bangkok 10330, Thailand

## Abstract

This paper presents a novel Transformer-based facial landmark localization network named Localization Transformer (LOTR). The proposed framework is a direct coordinate regression approach leveraging a Transformer network to better utilize the spatial information in the feature map. An LOTR model consists of three main modules: 1) a visual backbone that converts an input image into a feature map, 2) a Transformer module that improves the feature representation from the visual backbone, and 3) a landmark prediction head that directly predicts the landmark coordinates from the Transformer’s representation. Given cropped-and-aligned face images, the proposed LOTR can be trained end-to-end without requiring any post-processing steps. This paper also introduces the smooth-Wing loss function, which addresses the gradient discontinuity of the Wing loss, leading to better convergence than standard loss functions such as L1, L2, and Wing loss. Experimental results on the JD landmark dataset provided by the First Grand Challenge of 106-Point Facial Landmark Localization indicate the superiority of LOTR over the existing methods on the leaderboard and two recent heatmap-based approaches.

## 1 Introduction

Landmark localization focuses on estimating the positions of predefined key points in an image. For face landmark localization, these key points represent the different attributes of a human face, e.g., the contours of the face, eyes, nose, mouth, eyebrows, etc. Over the past decade, face recognition systems continue to leverage these landmarks for alignment, making face landmark localization an intrinsic part of these systems (An et al., 2020; Deng et al., 2018; Earp et al., 2021; Kumar et al., 2009; Liu et al., 2017; Parkhi et al., 2015; Schroff et al., 2015; Wang et al., 2018; Wolf et al., 2010). Additionally, face landmark localization aids in solving problems like face animation (e.g. Cao et al., 2013), 3D face reconstruction (e.g. Dou et al., 2017; Feng et al., 2018; Roth et al., 2015), synthesized face

detection (Yang et al., 2019), emotion classification (Day, 2016; Munasinghe, 2018), and facial action unit detection (Hinduja and Canavan, 2020). Given its wide range of applications, facial landmark localization is an essential area of research in computer vision. However, it is a challenging task owing to its dependency on variations in face pose, illumination and occlusion (Dibeklioglu et al., 2008; Earp et al., 2021).

Since its formulation, various statistical approaches have been proposed such as the Active Shape Model (ASM) (Cootes et al., 1995) and Active Appearance Model (AAM) (Cootes et al., 1998) to solve the face landmark localization problem. These models take in a prior information about a face (e.g., the face shape, texture etc) and then fine-tune the model parameters from the provided face

\*Email: uwatc@sertiscorp.com

†Contributed to this work during his internship at Sertis Vision Lab

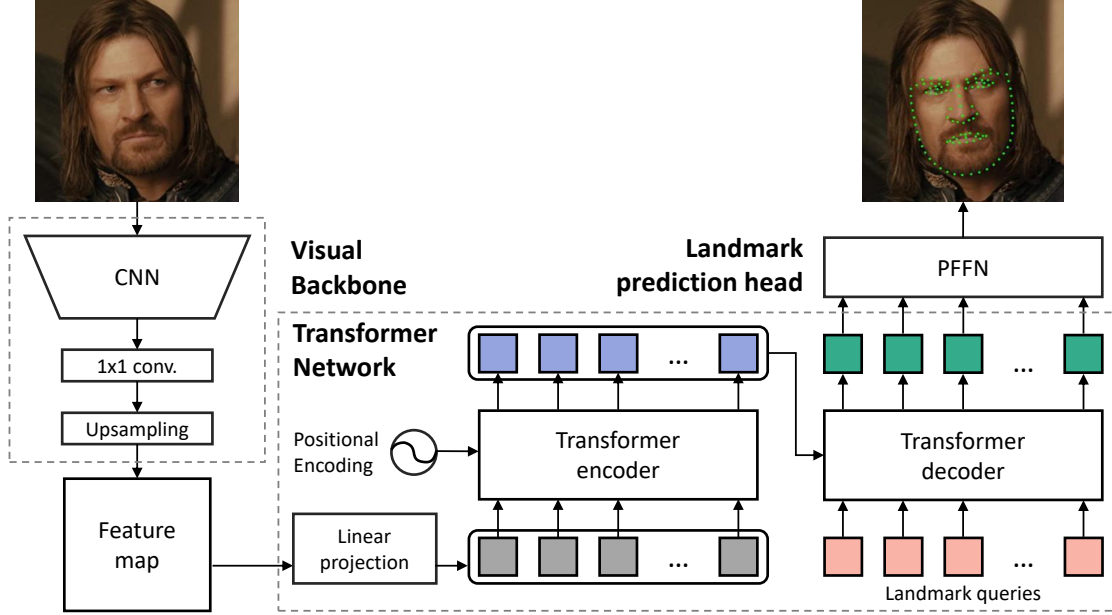


Figure 1: The overview of Localization Transformer (LOTR)

image. In addition, research has also been done in training patch-based detectors and component detectors to predict each landmark on local patches and anatomical components on the face image, respectively (Amberg and Vetter, 2011; Belhumeur et al., 2013; Efraty et al., 2011; Liang et al., 2008; Zhu and Ramanan, 2012a). However, due to the lack of global contextual information, these approaches require the best landmark configuration to be constrained on the face shape.

Since the early 2010s, researchers have developed different variants of Convolutional Neural Networks (CNNs), as an alternative to classical approaches, due to their ability to extract contextual information from an image. The two approaches, namely coordinate regression, and heatmap regression, are widely adopted with a CNN variant as a backbone.

In coordinate regression, a dense layer is added at the end of a CNN to predict each landmark’s coordinates. Notable works include Sun et al. (2013); Zhou et al. (2013), and Zhang et al. (2014a) which propose multi-level cascaded CNNs to localize facial landmarks. Combining coordinate regression along with multi-level cascaded CNNs has been instrumental in predicting the facial landmarks. In these frameworks, the early CNN levels aim to learn about the rough estimate of the landmarks, while the deeper levels seek to fine-tune the prediction. The main caveat of these approaches is the high architectural complexity, thereby increasing inference time. Recently, researchers have utilized multi-task learning to address this issue. Zhang et al. (2016) and Ranjan et al. (2016) propose lighter CNN architectures — robust to pose and occlusion — by combining the landmarks with the different attributes such as face detection, pose, facial expression, gender, etc. Ranjan et al. (2016) achieve a marginal reduction in error

for facial landmarks localization compared to Zhang et al. (2016). However, most regression-based approaches suffer from spatial information loss due to the compression of feature maps before the fully-connected layers (Earp et al., 2021).

Recently, heatmap-based approaches (e.g. Earp et al., 2021; Kowalski et al., 2017; Mahpod et al., 2018; Xiong et al., 2020) have extensively been used for face landmark localization tasks as they better utilize spatial information to boost the performance compared with coordinate regression methods. These methods predict spatial probability maps wherein each pixel is associated with the likelihood of the presence of a landmark location. Additionally, these approaches lead to better convergence than coordinate regression techniques and achieve state-of-the-art performance on multiple evaluation datasets. However, they rely on generating large heatmaps, increasing the post-processing complexity. Xiong et al. (2020) propose vectorization of predicted heatmaps and supervising training using vector labels obtained from a quasi-Gaussian distribution. This process helps reduce the post-processing complexity, in addition to their proposed method ranking second on the JD-landmark challenge (Liu et al., 2019). Earp et al. (2021) propose a heatmap regression approach that makes use of a bag of tricks and sub-pixel inference to surpass the performance of Xiong et al. (2020) on the JD-landmark challenge leaderboard (Liu et al., 2019). However, Xiong et al. (2020) and Earp et al. (2021) still rely on an external post-processing step to achieve the final landmark locations. This additional post-processing step increases computational complexity and thereby results in an increase in inference time (Earp et al., 2021) and, therefore, tackling this issue is the primary motivation behind this paper.

Although the coordinate regression methods mentioned so far may suffer from spatial information loss, they offer an end-to-end solution at a lower computational complexity than heatmap-based approaches. In this work, we re-investigate the direct coordinate regression approach for facial landmark localization but exploit a more sophisticated neural network architecture, i.e., the Transformers (Vaswani et al., 2017) to address the issue of spatial information loss. Transformer networks (Vaswani et al., 2017) are sequence transduction models comprising of an encoder-decoder architecture, utilizing attention mechanisms. With the scaling successes in natural language processing (NLP) achieved by Transformer, researchers have developed different variations of the Transformer framework for computer vision tasks. One such variant is the Detection Transformer (DETR) (Carion et al., 2020) which performs objection detection. Inspired by DETR, we propose a Transformer-based facial landmark localization network, named Localization Transformer (LOTR). As shown in Figure 1, LOTR consists of three main modules: 1) a visual backbone, 2) a Transformer network, and 3) a landmark prediction head. Firstly, LOTR adopts a CNN with optional upsampling layers to convert an input image into a feature map that is then reshaped to a sequence of tokens, each representing a pixel in the feature map. As mentioned earlier, CNN backbones exhibit better performance on vision tasks than classical methods by extracting image features. Furthermore, the Transformer module takes these features as sequence and fixed-length landmark queries as input and produces a sequence of tokens representing landmarks as output. Finally, the prediction head, a Position-wise Feed-Forward Network (PFFN), transforms each token into predicted landmark coordinates. Given cropped-and-aligned face images as input, the proposed LOTR can be trained end-to-end without requiring any post-processing step.

The key contributions of this research are summarized as follows:

- We propose a Transformer-based landmark localization network, named Localization Transformer (LOTR). To the best of our knowledge, this is the first research that investigates the use of Transformers in direct regression of landmarks.
- We demonstrate that the proposed LOTR framework detects facial landmarks accurately. Experimental results indicate the superiority of the proposed LOTR over other algorithms, such as two recent heatmap-based methods (Earp et al., 2021; Xiong et al., 2020), on the 1st JD-landmark localization challenge leaderboard (Liu et al., 2019).
- We further analyze the model size and computational complexity of the different variants of the LOTR framework. Comparing with a heatmap-based method (Earp et al., 2021) and a CNN-based direct coordinate regression method, the proposed LOTR outperforms both in terms of prediction accuracy, model size, and computational complexity.
- We also investigate the effect of standard loss functions on model training and propose a modified loss function, namely smooth-Wing loss, which addresses some issues in an existing loss function called the Wing loss (Feng et al., 2017). Experimental results show an improvement in performance for the LOTR models trained with the proposed smooth-Wing loss.

The remaining of this paper is organized as follows: Section 2 provides more detail of related work. Section 3 presents the proposed method, i.e., LOTR. Section 4 explains how experiments were setup and discusses the results. Section 5 concludes the paper.

## 2 Related Work

### 2.1 Direct coordinate regression

As discussed in Section 1, direct coordinate regression was widely adopted to solve landmark localization problems in the early research period. Regression-based approaches (e.g. Dong et al., 2018; Feng et al., 2017; Ranjan et al., 2016; Sun et al., 2013; Zhang et al., 2014a,b; Zhang et al., 2016) typically use a CNN along with a dense layer at the end to predict the landmark locations. Usually, for coordinate regression, the choice of loss is either mean-absolute error (L1 loss) or mean-squared error (L2 loss). Recently, Feng et al. (2017) introduce a new loss function called Wing loss for robust facial landmarks localization using regression, discussed in Section 2.5. Furthermore, Dong et al. (2018) use style-aggregated images from a generative adversarial module to train a facial landmark localization model along with the original image to increase the robustness of the variance of image styles.

Despite the advancement in regression-based techniques for landmark localization, spatial information loss remains one major drawback for this approach. This research addresses this limitation by replacing the dense layer at the end of a CNN backbone with a Transformer network to preserve spatial information by a positional encoding, discussed in Section 3.

### 2.2 Heatmap regression

As an alternative to coordinate regression methods, heatmap-fitting approaches tackle the spatial information loss issue by generating spatial probability maps. Spatial probability maps are heatmaps with pixel values corresponding to the probability of a landmark being in a certain location. Heatmap-fitting approaches (e.g. Kowalski et al., 2017; Kumar et al., 2020; Mahpod et al., 2018; Sun et al., 2019; Wu et al., 2018) have demonstrated state-of-the-art performance on facial landmark localization tasks.

A common practice for generating the ground-truth heatmaps is to compute the probability maps by fitting bivariate Gaussian density functions of relative offset values for each landmark, which is defined as:

$$G(x, y) = \exp \left[ -\frac{(x - x_0)^2 + (y - y_0)^2}{2\sigma^2} \right], \quad (1)$$

where  $(x, y)$  is the location on the heatmap and  $(x_0, y_0)$  represents the ground-truth coordinate of a landmark. The

simplest approach to extract the landmarks locations from these maps during inference is using the argmax operation. However, with the heatmap resolution being a limiting factor, recent approaches have proposed efficient ways to obtain sub-pixel localization (Xiao et al., 2018; Zhang et al., 2019). For instance, Zhang et al. (2019) propose the following formulation to obtain the landmarks from the predicted heatmaps using distribution fitting:

$$G(\mathbf{x}, \mu, \Sigma) = \frac{\exp(-\frac{1}{2}(\mathbf{x} - \mu)^T \Sigma^{-1}(\mathbf{x} - \mu))}{2\pi|\Sigma|^{\frac{1}{2}}}, \quad (2)$$

where  $\mathbf{x} = (x, y)$  is the location on the heatmap,  $\mu$  represents the estimated coordinate of the landmark, and  $\Sigma$  is the co-variance matrix between the  $x$  and  $y$  coordinates.

On the other hand, Earp et al. (2021) perform sub-pixel face landmark localization using intermittent shuffling of upsampling layers, sub-pixel inference, and a bag of tricks to achieve the second rank on the JD-landmark-2 validation set (Liu et al., 2019). While successfully preserving spatial information and achieving state-of-the-art performance on facial landmark localization tasks, heatmap regression methods suffer from high computational post-processing complexity in converting heatmaps into landmark coordinates.

Xiong et al. (2020) propose a vectorization approach where vector labels represent the ground-truth landmark positions using a quasi-Gaussian distribution. This proposed distribution is a Gaussian density function enhancing the distribution peak with an additional constant  $\theta$  while being bounded by a threshold  $3\sigma$ . This method also converts the predicted output heatmaps into vectors, which encode spatial information. This vectorization results in reduced sensitivity and post-processing complexity. However, like the other heatmap regression methods, this approach also hinders achieving an end-to-end pipeline requiring a post-processing step during inference.

### 2.3 Transformer-based heatmap approach

Lan et al. (2021) propose an approach that combines a Transformer encoder with heatmap regression. They mainly focus on reducing the quantization error that occurs from down-sampling operations. The authors name the proposed architecture Heatmap in Heatmap (HIH), which takes advantage of two heatmaps categories, namely the integer and decimal heatmaps. Integer heatmap is a probability map extracted from a CNN backbone, e.g., Stacked Hourglass Networks (Newell et al., 2016), which provide a rough spatial prediction for the landmark locations. On the other hand, decimal heatmaps give more fine-grained offset predictions. For each landmark location, decimal heatmaps fit bi-variate Gaussian density functions of relative offset values as in Equation 1. During inference, the final landmark locations, in both integer and decimal heatmaps, are computed from the maximum probability coordinates. The authors conduct experiments comparing two different architectures, namely a CNN and a Transformer encoder in combination with a CNN backbone. The proposed method outperforms the state-of-the-art algorithms (e.g. Feng et al., 2017; Kumar et al., 2020; Wang

et al., 2019; Wu et al., 2018) on WFLW-full (Wu et al., 2018) and COFW dataset (Burgos-Artiz et al., 2013). They also report that the HIH approach with a CNN yields more precise landmarks than a Transformer encoder.

Even though Lan et al. (2021) are the first who employ a Transformer encoder with heatmap regression to tackle facial localization problems, the main caveats of the heatmap regression approach, namely the post-processing complexity and the lack of an end-to-end pipeline, remain unaddressed.

### 2.4 DETR

Carion et al. (2020) propose a Transformer (Vaswani et al., 2017) framework for end-to-end object detection task. Their proposed DETECTION TRANSFORMER (DETR) framework achieves comparative performance to Faster R-CNN (Girshick et al., 2014) on the COCO dataset (Lin et al., 2014). The DETR framework performs the task of object detection by combining a CNN architecture with a Transformer. The architecture consists of a pre-trained CNN backbone, which extracts low-resolution feature maps from an input image. These feature maps are then converted into a sequence and fed to an encoder model, consisting of a Multi-Head Self-Attention (MHSA) module and a Feed-Forward Network (FFN). The Multi-Head Attention (MHA) module aims to find the relationship between input sequence tokens with each head computing "attention" by linearly projecting each token into query, key, and value vectors. Fixed positional encoding, which encodes the spatial positions of the learned features, is added to the input of each attention layer (Carion et al., 2020). The embeddings generated by the encoder are then fed to the decoder network which also uses MHSA mechanisms (Carion et al., 2020). The decoder model decodes the embeddings in parallel at each decoder layer. The decoder output is then fed into a fixed number of FFNs, also known as the prediction heads. Each prediction head consists of a class prediction and a predicted bounding box. The DETR model predicts all objects at once, computed in parallel. The authors train the model end-to-end using Hungarian loss to compare sets, performing bipartite matching between predicted and ground-truth objects.

Inspired by the DETR, we propose the Localization Transformer (LOTR), which predicts landmarks for the facial landmark localization task. The main difference between the two is that, unlike DETR, the LOTR does not have a class prediction head, and the attention mechanisms have a fixed number of queries as each input image has a fixed number of landmarks. Therefore, the LOTR models do not require the Hungarian loss and use direct coordinate regression in combination with a smooth-Wing loss for training the end-to-end pipeline.

### 2.5 Wing loss

Several loss functions have commonly been used to train landmark localization models, including L1 loss ( $L_1(x) = |x|$ ), and L2 loss ( $L_2(x) = \frac{1}{2}x^2$ ), and the smooth-L1 loss



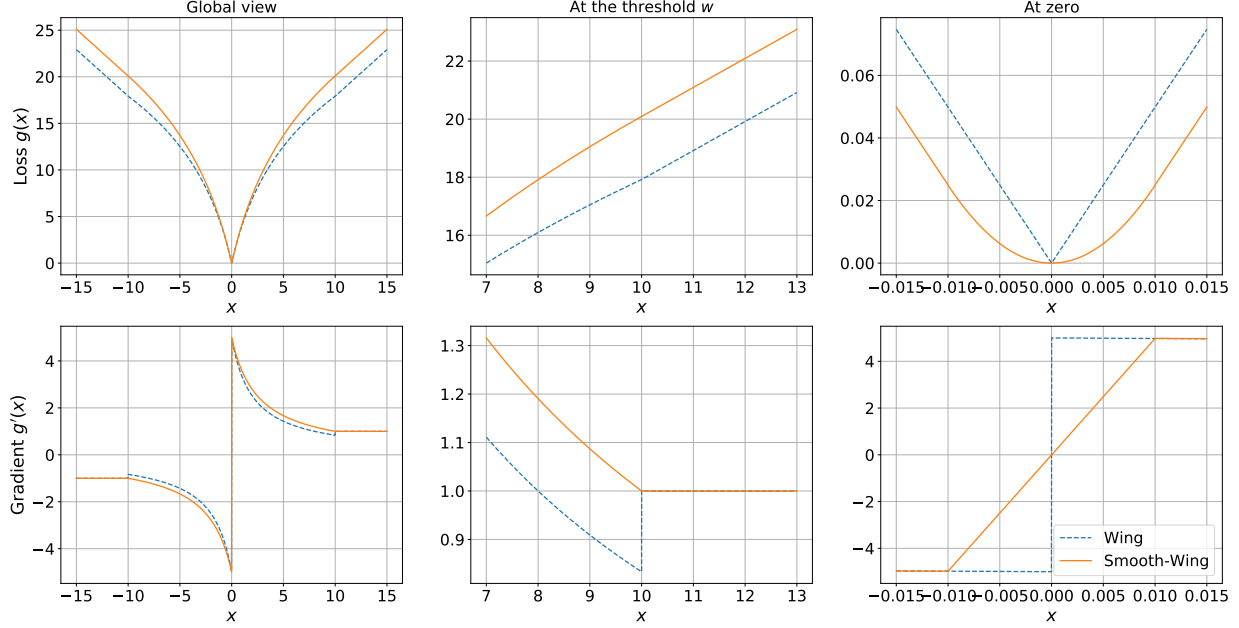


Figure 2: Comparison of Wing loss and smooth-Wing loss (top) and their gradient (bottom) in the global view (left), at the outer threshold  $w$  (middle), and at  $x$  equals zero (right). The parameters are set as follows:  $w = 10$ ,  $\epsilon = 2$ , and only for smooth-Wing,  $t = 0.01$ .

(Girshick, 2015), which is defined as:

$$\text{smooth-}L_1(x) = \begin{cases} \frac{1}{2}x^2 & \text{if } |x| < 1 \\ |x| - \frac{1}{2} & \text{otherwise.} \end{cases} \quad (3)$$

Feng et al. (2017) report another loss function—Wing loss—which is superior to other loss functions for landmark localization tasks. The key idea in the Wing loss is to force the model to pay more attention to small errors to improve the accuracy of the predicted landmarks. When prediction error is larger than a positive threshold, the Wing loss behaves like L1; otherwise, a logarithm function is used to compute the loss. It is defined as follows:

$$\text{wing}(x) = \begin{cases} w \ln(1 + \frac{|x|}{\epsilon}) & \text{if } |x| < w \\ |x| - c & \text{otherwise.} \end{cases} \quad (4)$$

where  $w$  is the threshold,  $\epsilon$  is a parameter controlling the steepness of the logarithm part, and  $c = w - w \ln(1 + w/\epsilon)$ .

However, as shown in Figure 2, the Wing loss produces the discontinuity of the gradient at the threshold  $w$ , as pointed out by Wang et al. (2019), and at zero error, which might affect the stability of training. In this work, we propose a modified Wing loss which is smooth everywhere and investigate its effectiveness.

### 3 Proposed methods

#### 3.1 Localization Transformer (LOTR)

This section explains in detail the proposed Transformer-based landmark localization network, named Localization Transformer (LOTR). Since LOTR is a coordinate regression approach that directly maps an input image into a set

of predicted landmarks, it requires neither heatmap representation nor any post-processing step. Figure 1 illustrates an overview of the architecture of the proposed LOTR framework. The LOTR model consists of three main modules, which include 1) a visual backbone, 2) a Transformer network, and 3) a landmark prediction head.

The visual backbone aims to capture context and extract features from an input image. The visual backbone takes an RGB image as input and produces a feature map as output. In this work, we exploit a pre-trained CNN such as MobileNetV2 (Sandler et al., 2018) or ResNet50 (He et al., 2016) to compute a feature map. We apply  $1 \times 1$  convolution to reduce the channel dimension of the feature map. Since the resolution of the feature map generated from the CNN backbone might be very low, e.g.,  $6 \times 6$  pixels for a  $192 \times 192$  input image, we optionally increase the resolution by using upsampling layers.

We then utilize a Transformer network (Vaswani et al., 2017) to enrich the feature representations while maintaining the global information in the feature map. As shown in Figure 1, the Transformer module is composed of a Transformer encoder and a Transformer decoder. Since Vaswani et al. (2017) designed Transformers to process sequential data, we convert the feature map  $\mathbf{F} \in \mathbb{R}^{W \times H \times C}$ , obtained from the visual backbone, into a sequence of tokens  $\mathbf{X} \in \mathbb{R}^{WH \times D}$ . In particular, we use a linear projection to reduce the channel dimension  $C$  of each pixel in  $\mathbf{F}$  to a smaller dimension  $D \leq C$ , followed by reshaping into a sequence of tokens.

A Transformer encoder, a stack of  $L$  encoder layers, then receives this sequence of tokens as input. Each en-

coder layer consists of two sublayers: 1) MHSA and 2) PFFN. Both these sublayers have residual connections and layer normalization applied to them. As mentioned in Section 2.4, the MHA established the relationship between tokens in the input sequence by computing the attention by linearly projecting each token into query, key, and value vectors and subsequently using the query and key vectors to calculate the attention weight applied to the value vectors. The output from the MHSA sublayer (the same size as its input) is then fed into PFFN to transform the input sequence’s representation further. These processes repeat  $L$  times using the output from the previous encoder layers as input. Similar to DETR (Carion et al., 2020), the LOTR adds 2D-positional encoding only to the query and key in each encoder layer. The output of the Transformer encoder is a transformed sequence  $\tilde{\mathbf{X}} \in \mathbb{R}^{W \times H \times D}$ , the same dimension as its input.

Following this encoding operation, the output from the Transformer encoder is then fed into a Transformer decoder, i.e., a stack of  $L$  decoder layers. Each decoder layer consists of three sublayers: 1) MHSA, 2) Multi-Head Cross-Attention (MHCA), and 3) PFFN. The first and the third are similar to those of the encoder layers. However, the input to the first sublayer of the first decoder layer is a sequence of landmark queries  $\mathbf{Y} \in \mathbb{R}^{N \times D}$ , each is an embedding of the same dimension  $D$ . The number of landmark queries equals  $N$ , which is the number of landmarks to predict. In this work, landmark queries are learnable parameters of LOTR, which are optimized during model training. The second sublayer, i.e., MHCA, takes the output of the first sublayer (MHSA) and the output generated by the encoder, i.e.,  $\tilde{\mathbf{X}}$ , as inputs, and then computes the relationship between each token between both sequences. The third sublayer, i.e., PFFN, then processes the output from the second sublayer. Like the Transformer encoder, all three of these sublayers have residual connections and layer normalization applied to them. The 2D-positional encoding is added to only the query and key in each layer. The Transformer decoder produces  $\tilde{\mathbf{Y}} \in \mathbb{R}^{N \times D}$  as output.

The landmark prediction head takes an embedding of the dimension  $D$  in the sequence  $\tilde{\mathbf{Y}}$  of length  $N$ , generated by the decoder as input, and produces as output  $\hat{\mathbf{Z}} \in \mathbb{R}^{N \times 2}$ , which stores the predicted the  $x$ - and  $y$ -coordinates of the  $N$  landmarks. This work exploits a simple PFFN with two hidden layers with ReLU activation. The output layer, however, which consists of only two nodes, is without any activation function.

### 3.2 Smooth-Wing loss

Since the proposed LOTR predicts a fixed number of landmarks ( $N$ ), a more complicated Hungarian loss used in DETR (Carion et al., 2020) is not required. The proposed LOTR can be trained end-to-end with a standard loss function given cropped-and-aligned face images as input. In particular, during the training phase, the predicted landmarks  $\hat{\mathbf{Z}}$  generated by LOTR are compared with the ground truth landmarks  $\mathbf{Z} \in \mathbb{R}^{N \times 2}$  to compute the loss, which is

defined as:

$$\text{loss}(\mathbf{Z}, \hat{\mathbf{Z}}) = \sum_{i=1}^N \sum_{j=1}^2 g(z_{ij} - \hat{z}_{ij}), \quad (5)$$

where the loss function  $g(x)$  can be any standard loss function such as L1, L2, smooth-L1, or Wing loss, which are described in Section 2.5. Although Feng et al. (2017) report the Wing loss to be superior to other loss functions for landmark localization, its major drawback is the gradient discontinuity at the threshold  $w$  and around the zero error (Figure 2). This discontinuity can affect the convergence rate and the stability of training.

In this work, we also propose a modified Wing loss, named smooth-Wing loss (s-wing( $x$ )), which is given by:

$$\text{s-wing}(x) = \begin{cases} sx^2 & \text{if } |x| < t \\ |x| - c_1 - c_2 & \text{if } |x| > w \\ (w + \epsilon) \ln(1 + \frac{|x|}{\epsilon}) - c_2 & \text{otherwise.} \end{cases} \quad (6)$$

where  $t$  is an additional threshold ( $0 < t < w$ ),  $s = (w + \epsilon)/(2t(\epsilon + t))$ ,  $c_1 = w - (w + \epsilon) \ln(1 + w/\epsilon)$ , and  $c_2 = st^2$ . When the error is smaller than the inner threshold  $t$ , it behaves like L2 loss, allowing the gradient to be smooth at zero error; otherwise, it behaves like the Wing loss. We define the constants  $s$ ,  $c_1$ , and  $c_2$  to smoothen the loss at the inner threshold  $t$  as well as at the outer threshold  $w$  (Figure 2).

## 4 Experiments

### 4.1 Datasets

We use the 106-point JD landmark dataset (Liu et al., 2019) to train and evaluate the proposed method. The dataset contains images from other face landmark datasets including as 300W (Sagonas et al., 2013; Sagonas et al., 2016), LFPW (Belhumeur et al., 2013), AFW (Zhu and Ramanan, 2012b), HELEN (Le et al., 2012), and IBUG (Sagonas et al., 2013), covering large variation of face pose and expression. These images are re-annotated with 106-point landmark, which provides more information about the face structure than any other face landmark datasets. The JD dataset consists of 11,393 images for training and 2,000 images each for validation and testing.

Following Earp et al. (2021), we use a ResNet50-based face detector, proposed by Deng et al. (2019), in our pre-processing step. In particular, we use the bounding box and a set of five simple landmarks (i.e., eye centers, nose tip, and mouth corners) obtained from the detector to crop and align the detected faces. We then resize the size of each input image to  $192 \times 192$  pixels before feeding it to our model. Earp et al. (2021) describe the pre-processing in more detail.

### 4.2 Evaluation metrics

We use the normalized mean error (NME), the failure rate, and the area under the curve (AUC) of the cumulative distribution as the metrics to evaluate and compare landmark

localization algorithms. The NME is computed across all predicted landmarks as follows:

$$\text{NME} = \frac{1}{N} \sum_{i=1}^N \frac{\|\mathbf{z}_i - \hat{\mathbf{z}}_i\|_2}{d}, \quad (7)$$

where  $N$  is the number of all landmarks,  $\mathbf{z}_i$  and  $\hat{\mathbf{z}}_i$  denotes the  $i$ -th ground truth landmark and the  $i$ -th predicted landmark, respectively, and  $d$  is a normalization factor. Following Liu et al. (2019), the normalization factor  $d$  is defined as  $\sqrt{W_{\text{bbox}} H_{\text{bbox}}}$ , where  $W_{\text{bbox}}$  and  $H_{\text{bbox}}$  are the width and height of the bounding box enclosing all the ground truth landmarks, respectively. If the NME of a test image is above a threshold, i.e., 8% (as defined by Liu et al. (2019)), it is considered as a failure. The failure rate is, therefore, the rate of failure cases. Liu et al. (2019) compute the AUC from the cumulative error distribution. It is a distribution where the proportion of all non-failure cases to the number of test images are plotted against the NME. Therefore, a larger AUC represents a more accurate algorithm.

### 4.3 Model training

Table 1 presents the configuration of three LOTR models, namely LOTR-M, LOTR-M+, and LOTR-R+, used in the experiments. The LOTR-M model is the base model that utilizes a MobileNetV2<sub>1.0</sub>, pretrained on the ImageNet dataset (Deng et al., 2009), as the visual backbone, generating a feature map of size  $6 \times 6 \times 1280$  from a  $192 \times 192$  RGB image. We reduce the number of feature channels to 64 by a  $1 \times 1$  convolution, then reshaping into a sequence of tokens. Subsequently, we use a Transformer module with two encoder layers and two decoder layers to process the sequence, followed by a dropout technique (Srivastava et al., 2014) with a dropout rate of 0.1. Following, we use a landmark prediction head, i.e., a PFFN consisting of two hidden layers with 512 nodes, with ReLU activation, followed by an output layer with two nodes, to process each token in the output sequence of the Transformer. In the LOTR-M+ model, to increase the resolution of the feature map, we insert upsampling layers between the MobileNetV2<sub>1.0</sub> backbone and the Transformer module. In particular, we utilize a  $1 \times 1$  convolution to reduce the number of channels to 256 and then apply two deconvolution layers (128 and 64 filters, with filter size =  $4 \times 4$ ) to increase the feature resolution to  $24 \times 24$  pixels, before feeding into the Transformer. The LOTR-R+ model adopt exactly the same configuration as LOTR-M+, except the backbone is changed to a pretrained ResNet50.

We initialize the parameters of the LOTR models using He’s method (He et al., 2015). We use a standard normal distribution to initialize the positional encoding and the landmark queries, both learnable. For the landmark queries, we specifically use a standard deviation of  $10^{-4}$  for the initialization. We train the LOTR models using the LAMB optimizer (You et al., 2019) with a base learning of  $10^{-3}$  for 100 epochs while reducing the learning rate with a factor of 0.1 at epochs 50 and 75 and setting the batch

size to 32. We use the smooth-Wing loss, described in Section 3.2, setting the inner threshold ( $t$ ) to 0.01, the outer threshold ( $w$ ) to 10, and the steepness control parameter ( $\epsilon$ ) to 2 as the parameters. For data augmentation and training tricks, we use the same steps described by Earp et al. (2021). We implement the model using MXNet framework (Chen et al., 2015) with Gluon libraries (Guo et al., 2020), using a single NVIDIA Titan X GPU for training.

Table 1: The architectures of LOTRs used in the experiments.

	LOTR-M	LOTR-M+	LOTR-R+
Backbone	MNetV2 <sub>1.0</sub>	MNetV2 <sub>1.0</sub>	ResNet50
$1 \times 1$ conv.	64	256	256
Upsampling	-	128, 64	128, 64
Transformer	2, 2	2, 2	2, 2
PFFN	512, 512, 2	512, 512, 2	512, 512, 2

### 4.4 Results on the JD-landmark dataset

Table 2 presents the performance of the proposed LOTR models, evaluated on the test set of the first Grand Challenge of 106-Point Facial Landmark Localization<sup>3</sup>. For brevity, the table includes only the result of the top two ranked algorithms out of 21 algorithms submitted to the challenge.

Table 2 shows that the proposed LOTR models, including the smallest model, LOTR-M gain more than 3% in the AUC in comparison to the top two ranking algorithms on the first challenge leaderboard. The table also compares LOTR models with two recent methods based on the heatmap regression, i.e., Earp et al. (2021) and Xiong et al. (2020). All of the proposed LOTR models surpass the heatmap approach in Xiong et al. (2020) by a significant amount of the AUC gain of 3.7–4.5%. When comparing with Earp et al. (2021), our LOTR models achieve better performance using the same backbone. While our smallest model LOTR-M is comparable with the ResNet50 model by Earp et al. (2021), our bigger models, i.e., LOTR-M+ and LOTR-R+, surpass it by an AUC gain of 0.15–0.65%, showing the superiority of our approach over theirs. Similar to Earp et al. (2021), we also utilize a flipping technique during inference to improve the prediction accuracy. In particular, we feed the original cropped-and-aligned face images and their horizontally flipped version into the model and average their corresponding predicted landmark coordinates.

### 4.5 Comparison with the heatmap regression approach

To study the effectiveness of using Transformer to reduce computational complexity by direct regression of coordinates, we measure and compare the inference speed with the heatmap approach model. We adopt a model from Earp et al. (2021) to be the baseline model since we followed

<sup>3</sup><https://facial-landmarks-localization-challenge.github.io>

Table 2: The evaluation results for different LOTR models on the JD-landmark test set<sup>3</sup>; † and ‡ denote the first and second place entries.

Model	AUC (%)	Failure rate (%)	NME (%)
LOTR-R+	87.71	0.00	0.98
LOTR-M+	87.21	0.00	1.02
Earp et al. (2021) (ResNet50)	87.06	0.00	1.03
LOTR-M	87.05	0.00	1.03
Earp et al. (2021) (MobileNetV2 <sub>1.0</sub> )	86.49	0.00	1.08
†Baidu-VIS	84.01	0.10	1.31
Xiong et al. (2020)	83.34	0.10	1.35
‡USTC	82.68	0.05	1.41

Table 3: Comparison of prediction accuracy, computational complexity, and model size.

Model	Backbone	AUC (%)		GPU (ms)		Size (MB)	Params ( $\times 10^6$ )
		No flip	Flip	No flip	Flip		
Earp et al. (2021)	MobileNetV2 <sub>1.0</sub>	85.24	86.49	24.74 $\pm$ 2.08	48.28 $\pm$ 3.20	12.16	2.92
	ResNet50	86.43	87.06	24.68 $\pm$ 1.51	50.99 $\pm$ 3.67	94.10	24.42
Earp et al. (2021) with vectorization	MobileNetV2 <sub>1.0</sub>	84.31	85.51	10.20 $\pm$ 1.45	18.90 $\pm$ 0.18	12.16	2.92
	ResNet50	84.65	85.94	11.12 $\pm$ 0.27	20.02 $\pm$ 0.35	94.10	24.42
CNN + FFN	MobileNetV2 <sub>1.0</sub>	85.85	86.37	5.51 $\pm$ 0.68	8.98 $\pm$ 1.95	14.71	3.89
	ResNet50	86.18	86.91	6.09 $\pm$ 0.90	9.86 $\pm$ 0.96	96.09	25.24
LOTR-M	MobileNetV2 <sub>1.0</sub>	86.39	87.05	5.46 $\pm$ 0.95	7.68 $\pm$ 1.08	10.59	2.81
LOTR-M+	MobileNetV2 <sub>1.0</sub>	86.56	87.21	5.63 $\pm$ 0.52	9.30 $\pm$ .81	14.03	3.71
LOTR-R+	ResNet50	87.09	87.71	6.00 $\pm$ 0.84	11.55 $\pm$ 1.03	95.97	25.21

the same pre-processing procedure, visual backbone, and the bag of tricks accordingly. We report the result in Table 3 where we run the model on a high computational CPU (Intel Xeon CPU E5-2698 v4) and NVIDIA Tesla V100 SXM2 32 GB.

In the pre-processing step, all the models use the same face detector by Deng et al. (2019) as mentioned in Section 4.1 with a processing time of  $43.36 \pm 4.82$  ms. Table 3 demonstrates the inference time reduction from the baseline on GPU by  $\sim 4\text{--}6\times$ , while maintaining a comparable model size and the number of parameters. Moreover, when considering the model with MobileNetV2<sub>1.0</sub> as a backbone, although LOTR-M and LOTR-M+ run with the flipping technique, the computational time is lower than Earp et al. (2021) (MobileNetV2<sub>1.0</sub>) without the flipping technique. This phenomenon is consistent with the larger visual backbone as well. Table 3 demonstrates that the LOTR-R+ model, with flipping technique, is  $\sim 4.4\times$  faster than MobileNetV2<sub>1.0</sub> model, with the flipping technique, in Earp et al. (2021) and  $\sim 2.1\times$  as fast as compared to the same without the flipping technique.

This experimentation demonstrates the complexity of the heatmap regression approach, where the model relies on a complicated post-processing procedure to generate spatial probability maps. Furthermore, some complex operations in post-processing may not utilize GPU acceleration, resulting in high computational time. In contrast,

the proposed LOTR models use a Transformer to directly regress the coordinates, which enables the model to reduce the computational time as it avoids complicated post-processing and is capable of utilizing GPU acceleration as the models consist of only simple operations.

Inspired by Xiong et al. (2020), we conduct another experiment incorporating vectorization and the band pooling module with the baseline approach (Earp et al., 2021). We analyze the effects on model performance and post-processing time reduction with vectorization. While the post-processing time significantly drops in converting heatmaps to vectorized labels and predictions, there is also a drop in performance. The Transformer-based approach, on the other hand, sees an increase in performance with a drop in the inference time, comparing to the baseline or the baseline with vectorization.

#### 4.6 Comparison with the Feed-Forward Network architecture

To investigate the significance of a Transformer’s ability in processing spatial features from the visual backbone, we compare its performance with a baseline CNN model with an FFN replacing the Transformer module. For a fair comparison, we apply a  $1 \times 1$  conv after retrieving the feature map from the visual backbone to resemble the spatial dimension of the LOTR models. We then use the FFN as a landmark prediction head to output the coordinates



of facial landmarks. For comparison purposes, we experiment with MobileNetV2<sub>1.0</sub> and ResNet50 as the visual backbones and adopt the same loss function and training tricks as described in Section 4.3.

According to the results presented in Table 3, the performance of the CNNs with FFN head are worse than LOTRs for both flip and no flip setups. This drop in performance may be due to the FFN lacking a mechanism to model complex relationships between spatial features.

In contrast, the Transformer architecture incorporates self-attention and cross-attention mechanisms to model this relationship. Moreover, landmark queries on the decoder side and the positional encoding might be why the LOTRs can encode abstract information of each landmark, resulting in an improved understanding of the models to perform direct regression. This shows that Transformer is more effective than FFN.

#### 4.7 Comparison of loss functions

In this section, we investigate the effect of the proposed smooth-Wing loss, as described in Section 3.2, by comparing it with standard loss functions (e.g., L1, L2, and smooth-L1) and Wing loss (Section 2.5). We conduct the experiment with the same training process described in Section 4.3. For the Wing loss, we set the threshold  $w = 10$  and  $\epsilon = 2$ .

Table 4 shows the results from different loss functions on the JD-landmark test set (Liu et al., 2019). The results from Table 4 show that LOTRs with L1 achieve comparable performance with smooth-L1, while with L2, the proposed models’ performance is worse than other loss functions. This result also coincides with the results from Feng et al. (2017). Unlike L1 loss, which maintains a constant gradient value across the error range, L2 produces a smaller gradient near zero, which causes the models to ignore small error values. Thus, L2 loss is sensitive to the outliers making it less responsive to comparatively small error values. Thus, models using L2 loss may end up omitting small errors, which may yield inaccurate predictions.

Table 4: Comparison of prediction accuracy (AUC) with different loss functions.

Model	LOTR-M	LOTR-M+	LOTR-R+
L2	84.52	84.28	86.73
L1	86.90	86.95	87.44
Smooth-L1	86.87	86.98	87.52
Wing	86.92	87.04	87.68
Smooth-Wing	<b>87.05</b>	<b>87.21</b>	<b>87.71</b>

Moreover, loss functions for landmarks localization—Wing and smooth-Wing—consistently outperform standard loss functions. The focus of these loss functions is on a small error range, which aids in precise landmark coordinates prediction.

Comparing Wing and the proposed smooth-Wing loss, LOTRs using the smooth-Wing loss function outperform the ones using Wing loss. This result shows the impact of training stability from smooth-Wing loss. Figure 2 shows an uneven gradient of Wing loss at the threshold  $w$  which

may not suitable for parameter adjustment. The proposed smooth-Wing loss smoothens the gradient at the threshold  $w$ , making training more stable and, thus, essential for parameter adjustment. Table 2 and 3 show that with the same visual backbone, our LOTRs with smooth-Wing loss outperform Earp et al. (2021). This establishes that training with the smooth-Wing loss helps the proposed LOTRs achieve state-of-the-art performance on the JD-landmark test set.

#### 4.8 The number of Transformer encoder/decoder layers

This section studies the impact of layers ( $L$ ) in both the Transformer encoder and the decoder. We experiment with the different values of  $L$  while keeping the other hyperparameters the same. Table 3 shows the results from the different numbers of encoder and decoder layers. The results show that the LOTR models with up to three layers can accurately localize landmarks and yield the highest AUC when  $L$  equals 2. The models become harder to optimize as the number of layers increases from three. The results of the deepest models, i.e.,  $L$  equals 6, is NaN, which might be a consequence of training instability when the number of layers becomes very large.

Figure 3: Comparison of prediction accuracy (AUC) based on varying number of Transformer layers.

Encoder/ decoder layers	LOTR-M	LOTR-M+	LOTR-R+
1	86.88	87.00	87.46
2	<b>87.05</b>	<b>87.21</b>	<b>87.71</b>
3	86.86	86.92	87.42
4	44.09	85.88	60.84
5	43.74	44.40	44.16
6	NaN	44.14	NaN

## 5 Conclusions

We show that our proposed LOTR-M, LOTR-M+, and LOTR-R+ outperform other algorithms, including the two current heatmap-based methods on the JD-landmark challenge leaderboard. Hence, proving that the Transformer-based direct coordinate regression is a promising approach for robust facial landmark localization.

We demonstrate how the proposed LOTR outperforms CNN models with FFN, trained under the same conditions. The results suggest an effective use of a Transformer network to improve the feature representation from a visual backbone. In contrast to other coordinate regression approaches that suffer from spatial information loss, our LOTRs utilize the crucial spatial information for landmark localization tasks.

We also show that the LOTRs are superior to the recently proposed heatmap-based method by Earp et al. (2021) in terms of accuracy and computational complexity. Since the proposed LOTR directly predicts the landmark coordinates, it avoids any computationally intensive post-processing required by the heatmap-based method, leading

to a  $\sim 4\text{-}6\times$  gain in speed at inference time. Although Xiong et al. (2020) exploit their proposed vectorization method to reduce the post-processing time, its downside is the reduction in prediction accuracy. The end-to-end training behavior of the LOTRs with smooth-Wing loss also leads to a better prediction performance when compared to the heatmap-based methods.

While Feng et al. (2017) report that their proposed Wing loss to be superior over other common loss functions such as L2, L1, and smooth-L1, we show that our proposed smooth-Wing loss leads to better optimized models. Because of its continuity of the gradients, using the smooth-Wing loss improves the training stability and convergence rate compared to the Wing loss.

## Acknowledgements

We are grateful to our colleagues Christina Kim, Jeff Hnybida, and Justin Cairns for their constructive input and feedback during the writing of this paper.

## References

- B. Amberg and T. Vetter. Optimal landmark detection using shape models and branch and bound. pages 455–462, 11 2011. doi: 10.1109/ICCV.2011.6126275.
- X. An, X. Zhu, Y. Xiao, L. Wu, M. Zhang, Y. Gao, B. Qin, D. Zhang, and Y. Fu. Partial FC: Training 10 million identities on a single machine. *arXiv e-prints*, art. arXiv:2010.05222, Oct. 2020.
- P. Belhumeur, D. Jacobs, D. Kriegman, and N. Kumar. Localizing parts of faces using a consensus of exemplars. *IEEE Transactions on Pattern Analysis and Machine Intelligence*, 35:2930–40, 12 2013. doi: 10.1109/TPAMI.2013.23.
- X. P. Burgos-Artizzu, P. Perona, and P. Dollar. Robust face landmark estimation under occlusion. In *Proceedings of the IEEE International Conference on Computer Vision (ICCV)*, December 2013.
- C. Cao, Y. Weng, S. Lin, and K. Zhou. 3d shape regression for real-time facial animation. 32(4), Jul 2013. ISSN 0730-0301. doi: 10.1145/2461912.2462012.
- N. Carion, F. Massa, G. Synnaeve, N. Usunier, A. Kirillov, and S. Zagoruyko. End-to-end object detection with transformers. In A. Vedaldi, H. Bischof, T. Brox, and J.-M. Frahm, editors, *ECCV (1)*, volume 12346 of *Lecture Notes in Computer Science*, pages 213–229. Springer, 2020. ISBN 978-3-030-58452-8.
- T. Chen, M. Li, Y. Li, M. Lin, N. Wang, M. Wang, T. Xiao, B. Xu, C. Zhang, and Z. Zhang. MXNet: A flexible and efficient machine learning library for heterogeneous distributed systems. *arXiv e-prints*, art. arXiv:1512.01274, Dec. 2015.
- T. Cootes, C. Taylor, D. Cooper, and J. Graham. Active shape models-their training and application. *Computer Vision and Image Understanding*, 61(1):38 – 59, 1995. ISSN 1077-3142. doi: https://doi.org/10.1006/cviu.1995.1004.
- T. F. Cootes, G. J. Edwards, and C. J. Taylor. Active appearance models. In *IEEE Transactions on Pattern Analysis and Machine Intelligence*, pages 484–498. Springer, 1998.
- M. Day. Exploiting facial landmarks for emotion recognition in the wild. *CoRR*, abs/1603.09129, 2016.
- J. Deng, W. Dong, R. Socher, L.-J. Li, K. Li, and L. Fei-Fei. ImageNet: A Large-Scale Hierarchical Image Database. In *CVPR09*, 2009.
- J. Deng, J. Guo, and S. Zafeiriou. Arcface: Additive angular margin loss for deep face recognition. *CoRR*, abs/1801.07698, 2018.
- J. Deng, J. Guo, Z. Yuxiang, J. Yu, I. Kotsia, and S. Zafeiriou. Retinaface: Single-stage dense face localisation in the wild. In *arxiv*, 2019.
- H. Dibeklioglu, A. A. Salah, and L. Akarun. 3d facial landmarking under expression, pose, and occlusion variations. In *2008 IEEE Second International Conference on Biometrics: Theory, Applications and Systems*, pages 1–6, 2008. doi: 10.1109/BTAS.2008.4699324.
- X. Dong, Y. Yan, W. Ouyang, and Y. Yang. Style aggregated network for facial landmark detection. *CoRR*, abs/1803.04108, 2018.
- P. Dou, S. K. Shah, and I. A. Kakadiaris. End-to-end 3D face reconstruction with deep neural networks. *Proceedings - 30th IEEE Conference on Computer Vision and Pattern Recognition, CVPR 2017*, 2017-January: 1503–1512, Apr 2017.
- S. W. Earp, A. Samacoits, S. Jain, P. Noinongyao, and S. Boonpunmongkol. Sub-pixel face landmarks using heatmaps and a bag of tricks. *arXiv preprint arXiv:2103.03059*, 2021.
- B. A. Efraty, M. Papadakis, A. Profitt, S. Shah, and I. A. Kakadiaris. Facial component-landmark detection. In *2011 IEEE International Conference on Automatic Face Gesture Recognition (FG)*, pages 278–285, 2011. doi: 10.1109/FG.2011.5771411.
- Y. Feng, F. Wu, X. Shao, Y. Wang, and X. Zhou. Joint 3D face reconstruction and dense alignment with position map regression Network. *Lecture Notes in Computer Science (including subseries Lecture Notes in Artificial Intelligence and Lecture Notes in Bioinformatics)*, 11218 LNCS:557–574, Mar 2018.
- Z.-H. Feng, J. Kittler, M. Awais, P. Huber, and X.-J. Wu. Wing loss for robust facial landmark localisation with convolutional neural networks. *Proceedings of the IEEE Computer Society Conference on Computer Vision and Pattern Recognition*, pages 2235–2245, Nov 2017.
- R. Girshick. Fast R-CNN. *arXiv e-prints*, art. arXiv:1504.08083, Apr 2015.
- R. Girshick, J. Donahue, T. Darrell, and J. Malik. Rich feature hierarchies for accurate object detection and semantic segmentation. In *Proceedings of the IEEE conference on computer vision and pattern recognition*, pages 580–587, 2014.

- J. Guo, H. He, T. He, L. Lausen, M. Li, H. Lin, X. Shi, C. Wang, J. Xie, S. Zha, A. Zhang, H. Zhang, Z. Zhang, Z. Zhang, S. Zheng, and Y. Zhu. Gluoncv and gluonnlp: Deep learning in computer vision and natural language processing. *Journal of Machine Learning Research*, 21 (23):1–7, 2020.
- K. He, X. Zhang, S. Ren, and J. Sun. Delving deep into rectifiers: Surpassing human-level performance on imagenet classification. In *2015 IEEE International Conference on Computer Vision (ICCV)*, pages 1026–1034, 2015. doi: 10.1109/ICCV.2015.123.
- K. He, X. Zhang, S. Ren, and J. Sun. Deep residual learning for image recognition. In *2016 IEEE Conference on Computer Vision and Pattern Recognition (CVPR)*, pages 770–778, 2016. doi: 10.1109/CVPR.2016.90.
- S. Hinduja and S. Canavan. Facial action unit detection using 3D facial landmarks. *arXiv e-prints*, art. arXiv:2005.08343, May 2020.
- M. Kowalski, J. Naruniec, and T. Trzcinski. Deep alignment network: A convolutional neural network for robust face alignment. *CoRR*, abs/1706.01789, 2017.
- A. Kumar, T. K. Marks, W. Mou, Y. Wang, M. Jones, A. Cherian, T. Koike-Akino, X. Liu, and C. Feng. Luvli face alignment: Estimating landmarks’ location, uncertainty, and visibility likelihood. *2020 IEEE/CVF Conference on Computer Vision and Pattern Recognition (CVPR)*, pages 8233–8243, 2020.
- N. Kumar, A. C. Berg, P. N. Belhumeur, and S. K. Nayar. Attribute and simile classifiers for face verification. In *2009 IEEE 12th International Conference on Computer Vision*, pages 365–372, 2009.
- X. Lan, Q. Hu, and J. Cheng. Hih: Towards more accurate face alignment via heatmap in heatmap. *arXiv preprint arXiv:2104.03100*, 2021.
- V. Le, J. Brandt, Z. Lin, L. Bourdev, and T. S. Huang. Interactive facial feature localization. *Computer Vision – ECCV 2012 Lecture Notes in Computer Science*, page 679–692, 2012.
- L. Liang, R. Xiao, F. Wen, and J. Sun. Face alignment via component-based discriminative search. pages 72–85, 10 2008. ISBN 978-3-540-88685-3.
- T.-Y. Lin, M. Maire, S. Belongie, L. Bourdev, R. Girshick, J. Hays, P. Perona, D. Ramanan, C. L. Zitnick, and P. Dollár. Microsoft COCO: Common Objects in Context. *arXiv e-prints*, art. arXiv:1405.0312, May 2014.
- W. Liu, Y. Wen, Z. Yu, M. Li, B. Raj, and L. Song. Sphreface: Deep hypersphere embedding for face recognition. *CoRR*, abs/1704.08063, 2017.
- Y. Liu, H. Shen, Y. Si, X. Wang, X. Zhu, H. Shi, Z. Hong, H. Guo, Z. Guo, Y. Chen, B. Li, T. Xi, J. Yu, H. Xie, G. Xie, M. Li, Q. Lu, Z. Wang, S. Lai, Z. Chai, and X. Wei. Grand challenge of 106-point facial landmark localization. *arXiv e-prints*, art. arXiv:1905.03469, May 2019.
- S. Mahpod, R. Das, E. Maiorana, Y. Keller, and P. Campisi. Facial landmark point localization using coarse-to-fine deep recurrent neural network. *arXiv*, abs/1805.01760, 2018.
- M. I. N. P. Munasinghe. Facial expression recognition using facial landmarks and random forest classifier. In *2018 IEEE/ACIS 17th International Conference on Computer and Information Science (ICIS)*, pages 423–427, 2018. doi: 10.1109/ICIS.2018.8466510.
- A. Newell, K. Yang, and J. Deng. Stacked hourglass networks for human pose estimation. *Lecture Notes in Computer Science (including subseries Lecture Notes in Artificial Intelligence and Lecture Notes in Bioinformatics)*, 9912 LNCS:483–499, Mar 2016. ISSN 16113349.
- O. M. Parkhi, A. Vedaldi, and A. Zisserman. Deep face recognition. In *Proceedings of the British Machine Vision Conference (BMVC)*, pages 41.1–41.12. BMVA Press, September 2015. ISBN 1-901725-53-7. doi: 10.5244/C.29.41.
- R. Ranjan, V. M. Patel, and R. Chellappa. Hyperface: A deep multi-task learning framework for face detection, landmark localization, pose estimation, and gender recognition. *CoRR*, abs/1603.01249, 2016.
- J. Roth, Y. Tong, and X. Liu. Unconstrained 3D face reconstruction. In *Proceedings of the IEEE Computer Society Conference on Computer Vision and Pattern Recognition*, volume 07-12-June-2015, pages 2606–2615. IEEE Computer Society, Oct 2015. ISBN 9781467369640. doi: 10.1109/CVPR.2015.7298876.
- C. Sagonas, G. Tzimiropoulos, S. Zafeiriou, and M. Pantic. 300 faces in-the-wild challenge: The first facial landmark localization challenge. In *2013 IEEE International Conference on Computer Vision Workshops*, pages 397–403, 2013. doi: 10.1109/ICCVW.2013.59.
- C. Sagonas, G. Tzimiropoulos, S. Zafeiriou, and M. Pantic. A semi-automatic methodology for facial landmark annotation. In *CVPR Workshops*, pages 896–903. IEEE Computer Society, 2013. ISBN 978-0-7695-4990-3.
- C. Sagonas, E. Antonakos, G. Tzimiropoulos, S. Zafeiriou, and M. Pantic. 300 faces in-the-wild challenge: database and results. *Image Vis. Comput.*, 47:3–18, 2016.
- M. Sandler, A. Howard, M. Zhu, A. Zhmoginov, and L.-C. Chen. MobileNetV2: Inverted residuals and linear bottlenecks. Jan 2018.
- F. Schroff, D. Kalenichenko, and J. Philbin. Facenet: A unified embedding for face recognition and clustering. *CoRR*, abs/1503.03832, 2015.
- N. Srivastava, G. Hinton, A. Krizhevsky, I. Sutskever, and R. Salakhutdinov. Dropout: A simple way to prevent neural networks from overfitting. *Journal of Machine Learning Research*, 15(56):1929–1958, 2014.
- K. Sun, Y. Zhao, B. Jiang, T. Cheng, B. Xiao, D. Liu, Y. Mu, X. Wang, W. Liu, and J. Wang. High-resolution representations for labeling pixels and regions. *arXiv*, abs/1904.04514, 2019.

- Y. Sun, X. Wang, and X. Tang. Deep convolutional network cascade for facial point detection. In *2013 IEEE Conference on Computer Vision and Pattern Recognition*, pages 3476–3483, 2013. doi: 10.1109/CVPR.2013.446.
- A. Vaswani, G. Brain, N. Shazeer, N. Parmar, J. Uszkoreit, L. Jones, A. N. Gomez, Ł. Kaiser, and I. Polosukhin. Attention is all you need. Technical report, 2017.
- H. Wang, Y. Wang, Z. Zhou, X. Ji, Z. Li, D. Gong, J. Zhou, and W. Liu. Cosface: Large margin cosine loss for deep face recognition. *CoRR*, abs/1801.09414, 2018.
- X. Wang, L. Bo, and L. Fuxin. Adaptive wing loss for robust face alignment via heatmap regression. *Proceedings of the IEEE International Conference on Computer Vision*, pages 6970–6980, Apr 2019.
- L. Wolf, T. Hassner, and Y. Taigman. Similarity scores based on background samples. In H. Zha, R.-i. Taniguchi, and S. Maybank, editors, *Computer Vision – ACCV 2009*, pages 88–97, Berlin, Heidelberg, 2010. Springer Berlin Heidelberg. ISBN 978-3-642-12304-7.
- W. Wu, C. Qian, S. Yang, Q. Wang, Y. Cai, and Q. feng Zhou. Look at boundary: A boundary-aware face alignment algorithm. *2018 IEEE/CVF Conference on Computer Vision and Pattern Recognition*, pages 2129–2138, 2018.
- B. Xiao, H. Wu, and Y. Wei. Simple baselines for human pose estimation and tracking. *arXiv*, abs/1804.06208, 2018.
- Y. Xiong, Z. Zhou, Y. Dou, and Z. Su. Gaussian vector: An efficient solution for facial landmark detection. *arXiv preprint arXiv:2010.01318*, 2020.
- X. Yang, Y. Li, H. Qi, and S. Lyu. Exposing gan-synthesized faces using landmark locations. *CoRR*, abs/1904.00167, 2019.
- Y. You, J. Li, S. Reddi, J. Hseu, S. Kumar, S. Bhojanapalli, X. Song, J. Demmel, K. Keutzer, and C.-J. Hsieh. Large batch optimization for deep learning: Training BERT in 76 minutes. Technical report, 2019.
- F. Zhang, X. Zhu, H. Dai, M. Ye, and C. Zhu. Distribution-aware coordinate representation for human pose estimation. *arXiv preprint arXiv:1910.06278*, 2019.
- J. Zhang, S. Shan, M. Kan, and X. Chen. Coarse-to-fine auto-encoder networks (cfan) for real-time face alignment. In D. Fleet, T. Pajdla, B. Schiele, and T. Tuytelaars, editors, *Computer Vision – ECCV 2014*, pages 1–16, Cham, 2014a. Springer International Publishing. ISBN 978-3-319-10605-2.
- Z. Zhang, P. Luo, C. C. Loy, and X. Tang. Facial landmark detection by deep multi-task learning. In *European Conference on Computer Vision*, pages 94–108. Springer, 2014b.
- Z. Zhang, P. Luo, C. C. Loy, and X. Tang. Learning deep representation for face alignment with auxiliary attributes. *IEEE Transactions on Pattern Analysis and Machine Intelligence*, 38(5):918–930, 2016. doi: 10.1109/TPAMI.2015.2469286.
- E. Zhou, H. Fan, Z. Cao, Y. Jiang, and Q. Yin. Extensive facial landmark localization with coarse-to-fine convolutional network cascade. In *2013 IEEE International Conference on Computer Vision Workshops*, pages 386–391, 2013. doi: 10.1109/ICCVW.2013.58.
- X. Zhu and D. Ramanan. Face detection, pose estimation, and landmark localization in the wild. In *2012 IEEE Conference on Computer Vision and Pattern Recognition*, pages 2879–2886, 2012a. doi: 10.1109/CVPR.2012.6248014.
- X. Zhu and D. Ramanan. Face detection, pose estimation, and landmark localization in the wild. In *2012 IEEE Conference on Computer Vision and Pattern Recognition*, pages 2879–2886, June 2012b. doi: 10.1109/CVPR.2012.6248014.